18th Brazilian Congress of Thermal Sciences and Engineering
November 16-20, 2020 (Online)

ENC-2020-0207
EXPERIMENTAL STUDY AND MASS CHARGE SIMULATION MODEL IN A DIRECT EXPANSION SOLAR ASSISTED HEAT PUMP CHARGED WITH CO_2

Gleberson Marques Humia
Postgraduate Program in Mechanical Engineering (PPGMEC) - Federal University of Minas Gerais (UFMG), Av. Antônio Carlos 6627, Pampulha, 31.270-901, Belo Horizonte, MG, Brazil.
ghumia@ufmg.br mails

Willian Moreira Duarte
Postgraduate Program in Mechanical Engineering (PPGMEC) - Federal University of Minas Gerais (UFMG), Av. Antônio Carlos 6627, Pampulha, 31.270-901, Belo Horizonte, MG, Brazil.
University Center of Belo Horizonte (UniBH), Av. Prof. Mário Werneck, 1685, Estoril, 30575-180, Belo Horizonte, MG, Brazil.
willianmoreiraduarte@gmail.com

Juan Jose Garcia Pabon
Institute of Mechanical Engineering, Federal University of Itajubá, Av. BPS 1303, 37.500-903, Pinheirinho, Itajubá, MG, Brazil.
langa_27@hotmail.com

Sabrina Nogueira Rabelo Ruas
University of Itaúna, School of Mechanical Engineering, Highway MG 431, Itaúna/Pará de Minas interchange, 35680-142, Itaúna, MG, Brazil.
sasanogueirarab@hotmail.com

Tiago de Freitas Paulino
Graduate Program in Mechanical Engineering, Federal Center for Technological Education of Minas Gerais (CEFET-MG), Av. Amazonas, 5253, Nova Suíça, 30421-169, Belo Horizonte, MG, Brazil.
tfpaulinoeng@gmail.com

Luiz Machado
Postgraduate Program in Mechanical Engineering (PPGMEC) - Federal University of Minas Gerais (UFMG), Av. Antônio Carlos 6627, Pampulha, 31.270-901, Belo Horizonte, MG, Brazil.
luizm@ufmg.br

Abstract. *The present work is a theoretical/experimental study about the fluid mass charge in a direct expansion solar assisted heat pump (DX-SAHP), for the supply of domestic hot water. The heat pump operates in the transcritical cycle, with carbon dioxide as the refrigerant. CO_2 is a natural fluid that has an ozone depletion potential (ODP) equal to zero and a global warming potential (GWP) equal to one. For the heat pump to operate with high-energy efficiency, it is essential to know the CO_2 mass charge to be used under various conditions of insolation. The effects of solar radiation changes were analyzed in 48 experimental points, evaluated under three different conditions of mass. The results were compared with a simulation model that used eight void fraction correlations for the two-phase flow of the solar evaporator. To estimate the amount of mass in each part of the heat pump, the phenomena of heat transfer and head loss were considered in the model, both in the evaporator and in the gas cooler, as well as the conditions of the fluid in the supercritical region. The best results for mass prediction were obtained by the correlations of Hughmark and Filimonov, with an average error in absolute terms of 5.53% and 6.03% respectively. Considering a tolerance margin of ± 2%, the Hughmark correlation generated a total accuracy of 27.1% of the predictions against 14.6% achieved by the correlations of Zivi, Premoli and Filimonov. All the correlations tested were 100% correct for a tolerance of ± 18%.*

Keywords: *Heat Pump; CO_2; Void fraction; Fluid mass charge; Simulation Model.*

1. INTRODUCTION

CO_2 (R-744) was one of the first refrigerant fluids applied to refrigeration systems and was widely used in the 20th century until the mid-1930s. With the advent of CFCs and HCFCs, CO_2 was losing market until it was almost not used in

the early 1960s. With environmental problems and the establishment of the Montreal and Kyoto Protocols, CO_2 has reappeared as a promising alternative to be used in many applications in the various refrigeration sectors.

It is a natural, non-toxic, non-flammable, non-corrosive fluid, compatible with various lubricating oils, with a high volumetric capacity, low-pressure ratio, high heat exchange coefficients and mainly a low environmental impact, with zero ODP and GWP equal to 1. It works close to the critical point (31.04°C and 73.82 bars), which added to its high vapor pressure ends up affecting its density, both in the subcritical and supercritical conditions, being an important factor to be considered in mass forecasting models. According to Islam et al. (2012), CO_2 operating in a transcritical cycle is the refrigerant that presents one of the best perspectives in relation to the TEWI index.

Revellin (2009) points to the effect of the amount of refrigerant fluid loaded on a refrigeration machine in relation to its performance, so there is an optimum amount of fluid that will generate less energy consumption. Studies of effects of refrigerant charge in a DX-SAHP is presented by Kong *et al* (2017) and Zhang *et al* (2014), in both studies a charge of refrigerant is recommend for maximization of the COP. Aprea (2015) also mentions that the performance of the transcritical system is more sensitive to the amount of refrigerant charge than a conventional air conditioner and its performance is critically linked to an appropriate mass charge, which strongly affects exergy loss in the compressor.

The main objective of this work is the development of a simulation model based on the use of several void fraction correlations to estimate the amount of refrigerant mass distributed among the components of a direct expansion solar assisted heat pump operating with CO_2. For model validation, experimental tests were carried out in order to measure the real value of the equipment's refrigerant mass.

2. EXPERIMENTAL DEVICE

The experimental device used in this work is a Direct Expansion Solar Assisted Heat Pump (DX-SAHP), as shown in Fig. 1. In this type of configuration, the evaporator itself is used as a solar collector and developed to absorb the solar radiation (direct and diffuse), the energies provided by air convection (natural or forced), and the condensation of atmospheric water vapor.

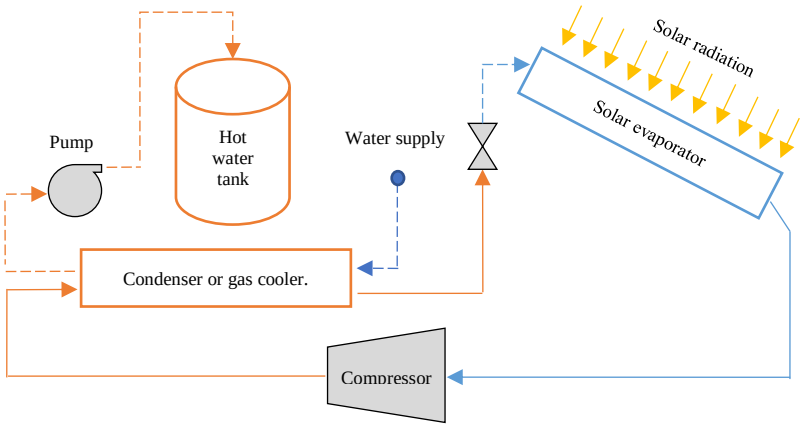

Figure 1. Basic diagram of a DX-SAHP heat pump.

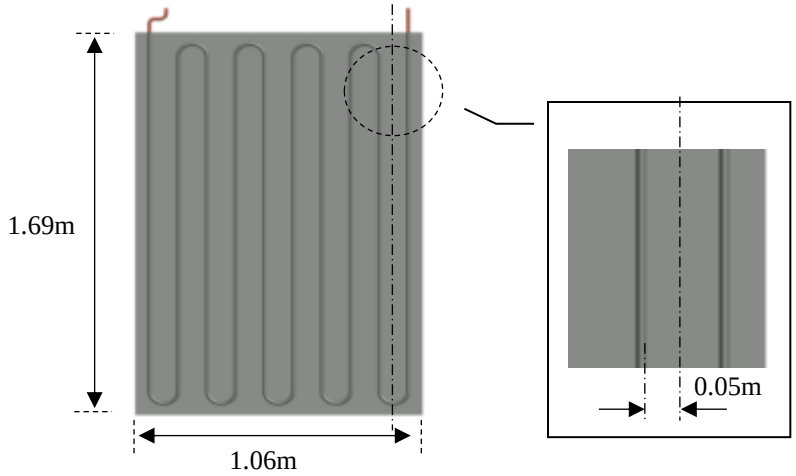

Figure 2. Basic diagram of a DX-SAHP heat pump.

2.1. Description of the main components

The solar evaporator of the heat pump consists of a copper tube arranged in the form of a serpentine, coupled to a flat copper plate as shown in Fig. 2, and mounted at an angle of inclination of 21°.

The gas cooler is a counter-current concentric tube heat exchanger, in which the primary fluid (CO_2) circulates in the inner tube and the secondary fluid (H_2O) circulates in the annular region. The tube is wrapped in a spiral shape around an insulated PVC tank with polyurethane foam.

The equipment consists of a hermetic reciprocating compressor with constant speed, displacement of 1.75 cm³/rot and driven by an asynchronous two-pole electric motor, brand SADEN, model # 6455 110-127 VAC R744 G319 SRCaDB. Its expansion device is a needle-type valve, model SS-31RS4, manufactured by SWAGELOK, with an orifice diameter of 1.6mm. The heat pump also has a liquid separator, an oil separator, as well as a pump for circulating water through the gas cooler. Table 1 presents a summary of the dimensional characteristics of the equipment.

Table 1. Dimensional characteristics of the heat pump.

Item	Description	Identification	Length [m]	Diameter [mm]	Volume [m^3]
1	Compressor	Internal volume	-	-	$1.75x10^{-6}$
2	Pipe	Connection between compressor and oil separator	0.620	4.66	$1.06x10^{-5}$
3	Oil separator	Internal volume - manufacturer data	0.165	73.00	$6.91x10^{-4}$
4	Pipe	Connection between oil separator and gas cooler	2.010	4.66	$3.43x10^{-5}$
5	Gas cooler	Inner piping	24.300	6.00	$6.87x10^{-4}$
6	Pipe	Connection between the gas cooler and the thermostatic valve	2.845	4.66	$4.85x10^{-5}$
7	Pipe	Connection between the thermostatic valve and the evaporator	0.180	4.66	$3.07x10^{-6}$
8	Evaporator	Pipe	16.300	4.66	$2.78x10^{-4}$
9	Pipe	Connection between evaporator and liquid separator	1.000	4.66	$1.71x10^{-5}$
10	Liquid separator	Internal volume - manufacturer data	0.215	90.00	$1.37x10^{-3}$
11	Pipe	Connection between liquid separator and compressor	1.115	4.66	$1.90x10^{-5}$

2.2. Instrumentation

The heat pump is equipped with several sensors, including seven thermocouples (T), four pressure transducers (P), two pyranometers (I), and one active power meter (J). All sensors are coupled to a data acquisition system connected to an interface programmed in LabVIEW ®. The distribution of the sensors follows the configuration of Fig. 3, and the measurement uncertainties associated with the measured quantities and their instruments are shown in Tab. 2.

Table 2. Measurement uncertainties.

Physical quantity	Instrument	Uncertainty	Unity	Note
Pressure	Zurich Transmitter	± 0.2	bar	1% scale background (10 to 40°C)
Pressure	FuelTech Transmitter	± 0.2	bar	0,5% scale background
Temperature	T-type thermocouple	± 0.8	°C	-59°C to 93°C
Solar irradiation	Pyranometer	2%	W/m^2	---
Mass	Weighing scales	± 5	g	---
Length	Pachymeter	± 0.02	mm	Resolution 1/50 mm
Length	Metric tape	± 1	mm	Resolution 1/2 mm
Volume	Beaker	± 0.2	ml	Resolution 0.2 ml
Electric power	Active Power Meter	5%	W	---

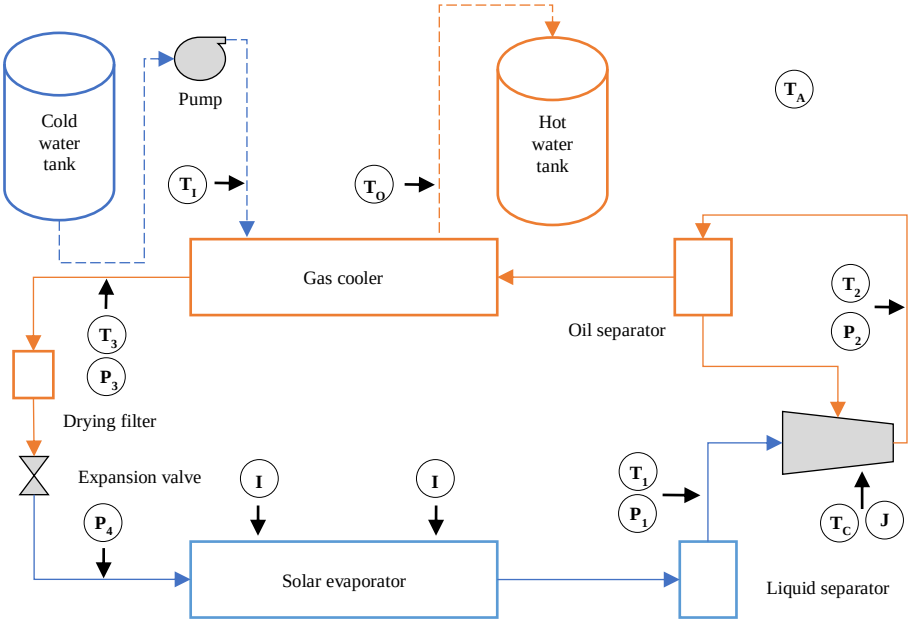

Figure 3. Schematic drawing of the sensors installed in the DX-SAHP.

3. MATHEMATICAL MODEL

To calculate the total fluid mass in each part of the equipment, a mathematical model for simulating the heat pump was implemented using the software EES - Engineering Equation Solver. In Item 7 it is possible to see the nomenclature used in this work.

Geometrical data for each section of the heat pump are provided as input parameters for the model, including the volumes or lengths and internal diameters of the piping of each corresponding section. The readings obtained by the sensors shown in Fig. 3 are also provided, as well as the volumetric flow rate of the water pump.

Based on the input parameters and considering the effect of the pressure drop along the pipes of the solar evaporator and the gas cooler, the thermodynamic properties of the fluid can be obtained. The mass flow rate of the refrigerant can then be determined by means of an energy balance between the primary and secondary fluids, according to Eq. 1.

$$\dot{m}_{CO2}(h_2 - h_3) = \dot{m}_w c_{p,\mathrm{w}}\left(T_{\mathrm{w,o}} - T_{w,\mathrm{i}}\right) \tag{1}$$

To calculate the length of the evaporator's single-phase region, the model considers a balance between the energy collected by the evaporator (solar irradiation, convection, radiation and condensation), with the energy supplied to the refrigerant, according to Eq. 2.

$$\dot{m}(h_o - h_i) = H_{in}\pi d_{in} L_0\left(T_{wall,in} - T_{av}\right) \tag{2}$$

The average temperature of the external wall in the control volume $T_{wall,ex}$ can be obtained by Fourier's Law through the conduction of heat in the pipe wall by Eq. 3.

$$\dot{Q}_n = \frac{2\pi L_o k\left(T_{wall,ex} - T_{wall,in}\right)}{\ln d_{in}/d_{ex}} \tag{3}$$

The external heat transfer coefficient by natural convection H_{conv} can be calculated using the correlation of Churchill and Chu (1975). The condensation heat transfer coefficient H_{cond} is determined according to Çengel (2015), using the model of Nusselt (1916) modified by Rohsenow (1956).

Because the evaporator is mounted on a metallic surface, the heat transfer can be calculated based on a finned surface, following the methodology proposed by Duffie and Beckman (2013). The total heat transfer rate in each control volume $\dot{Q}_n$, is then calculated by the composition between the convection, condensation, and radiation rate, $\dot{Q}_{conv}$, $\dot{Q}_{cond}$ and $\dot{Q}_{rad}$ respectively, in addition to the effect of solar irradiation on Eq. 5, where *S* represents the net radiation absorbed by the collector.

$$\dot{Q}_n = \dot{Q}_{conv} + \dot{Q}_{cond} + \dot{Q}_{rad} \tag{4}$$

$$\dot{Q}_{conv} = H_{conv}\eta A_t\left(T_\infty - T_{wall,ex}\right) + SA_t \quad (5)$$

$$\dot{Q}_{cond} = H_{cond}A_t\left(T_\infty - T_{wall,ex}\right) \quad (6)$$

$$\dot{Q}_{rad} = A_t\sigma_{SB}\varepsilon\left({T_\infty}^4 - {T_{wall,ex}}^4\right) \quad (7)$$

The head loss along the two-phase flow section is determined based on the Collier Equation (1972), using the separated-phases model of Lockhart and Martinelli (1949). Since in the two-phase flow the temperature of the external wall is uniform and practically constant throughout the evaporator, the heat transfer, by either radiation, convection, condensation or irradiation can also be considered uniform and constant. Rice (1987) mentions that in this case, the length of the control volume can be found considering Newton's Law of Cooling, represented by Eq. 8.

$$\dot{Q}_n = H_n\pi d_n L_n\left(T_{wall,in} - T_m\right) \quad (8)$$

The value of the void fraction is calculated for each volume control, considering the correlations of Homogeneous Model, Zivi (1964), Domansky and Didion (1983), Premoli (1971), Hughmark (1965), Rouhani modified by Steiner (1992), Melkamu (2007) and Filimonov's correlation (1957). Then, the mass value can finally be found along the two-phase flow section.

The mass of the superheated steam region is calculated by the average density of the fluid in that region. In the evaporator, the total mass is determined by the sum of the two-phase region and the superheat region masses.

In the gas cooler, the mathematical model determines the heat transfer rate in the super dense liquid and by means of a local energy balance with the secondary fluid, shown in Eq. 9, the water temperature $T_{\mathrm{w,Tc}}$ is obtained at the point that coincides with the beginning of the supercritical fluid region.

$$\dot{m}(h_{Tc} - h_3) = \dot{m}_w c_{p,\mathrm{w}}\left(T_{w,\mathrm{Tc}} - T_{\mathrm{w},1}\right) \quad (9)$$

In the supercritical region, the global heat transfer coefficient U can be found from the water and the refrigerant heat transfer coefficients, obtained respectively, with the correlations of Gnielinski (1976) and Yoon (2003). Thus, through Eq. 10, it is possible to determine the heat transfer area as well as the length of the supercritical region.

$$\dot{Q}_{sd} = UA\Delta T_m \quad (10)$$

Found the length of supercritical region and knowing the total length of the gas cooler, it is possible to determine the length of the super dense region. As this region is relatively small, the model calculates its mass directly from the average density of the fluid in that region. For the supercritical region, its length is divided into control volumes, determining the average density of each volume and calculating the total fluid mass in that region.

The calculation of the mass in the pipes and other accessories of the heat pump are made based on the average density of the fluid in each accessory. The mathematical correlations used in this work is listed in appendices 1.

4. RESULTS

As shown in Fig. 4, the compressor (T1) and evaporator (T4) inlet temperatures have a similar behavior in relation to the low-pressure, increasing when the solar irradiation increases, and decreasing when it decreases. The same behavior can be observed with the overheating of the refrigerant fluid at the outlet of the solar evaporator. Since the power required by the compressor is practically constant, as the compressor inlet temperature (T1) decreases due to the reduction of irradiation, it is seen that the compressor outlet temperature (T4) also decreases. As for the gas cooler outlet temperature (T3), it is observed that as expected, it is not influenced by the level of irradiation.

With respect to the pressure cycle, can be seen in Fig. 5 that the high-pressure in the gas cooler practically does not change with the variation of the solar radiation. This is because the water inlet and outlet temperatures remain practically constant and the opening of the expansion device is kept fixed during the tests. As for the pressure in the evaporator, it increases with the increase in solar irradiation, which in fact was already expected.

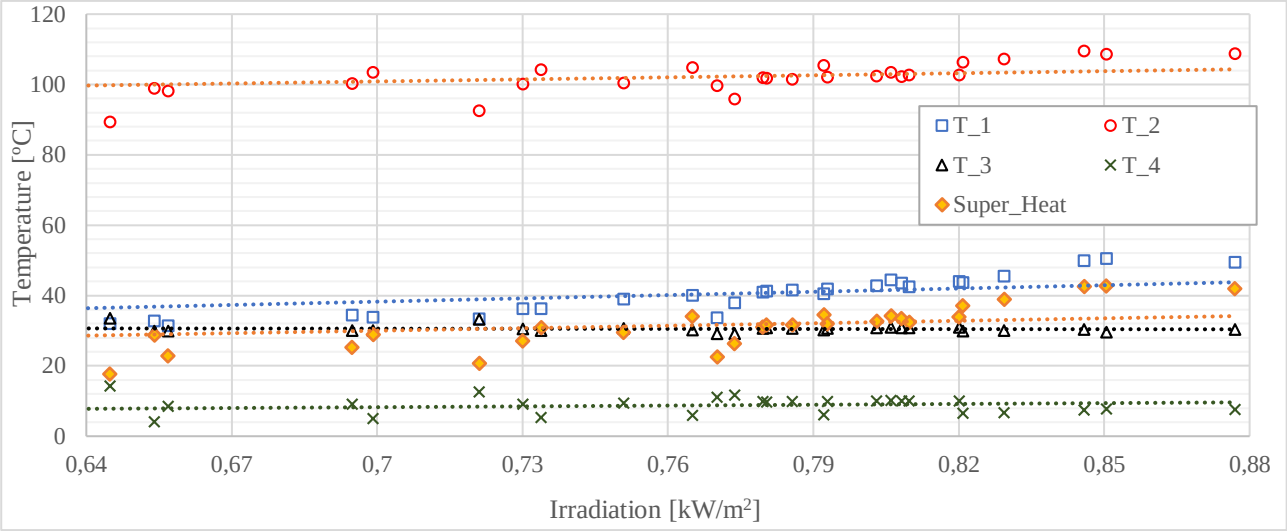

Figure 4 – Cycle temperatures as a function of solar irradiation.

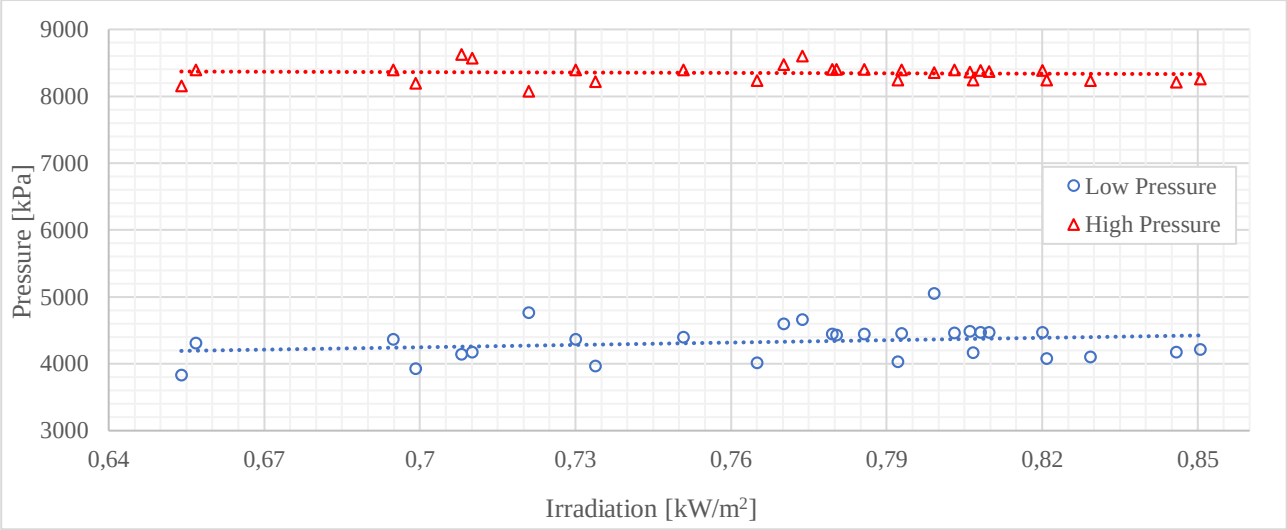

Figure 5 – Cycle pressures as a function of solar irradiation.

Figure 6 presents the results of the total mass obtained by the simulation model for each experimental operation point as a function of solar irradiation. Initially, the results can be separated by the presence or absence of solar radiation; thus, points 12 to 18 and 32 to 35 were obtained in the shade and the others in sunlight. It is noted that the mass obtained in the shade test shows lower results than those obtained under the sun. As noted in Fig. 4 and 5, when the evaporator is exposed to the sun, temperatures and pressures tend to be higher. The increased temperature results in decreased density of the refrigerant, however, the increased pressure causes an opposite effect, being the most significant and causing an increase in the density of the fluid in the compressor suction and, hence, increased overall mass.

It is also noticed that in Fig. 6, for the same experimental mass value, the increase in irradiation causes the decrease in the total mass calculated by the model. This result can be explained by the behavior of the density of CO_2 in the supercritical region. As already noted in Fig. 7 and 8, the temperature at the compressor outlet (T2) tends to increase with increasing irradiation, resulting in a decrease in the density of the fluid, nevertheless, the pressure at that point remains constant. Montagner (2013) mentions that variations in pressure and temperature in the supercritical region substantially affect the density of CO_2, especially near the critical point. Thus, in the range of working pressures observed in the gas cooler, around 8200 kPa, small temperature variations result in considerable variations in its density. On the other hand, as already explained, the increase in radiation causes an increase in the density in the evaporator, which would increase the total mass of the system, however, this effect is overcome by the decrease in mass in the high-pressure region.

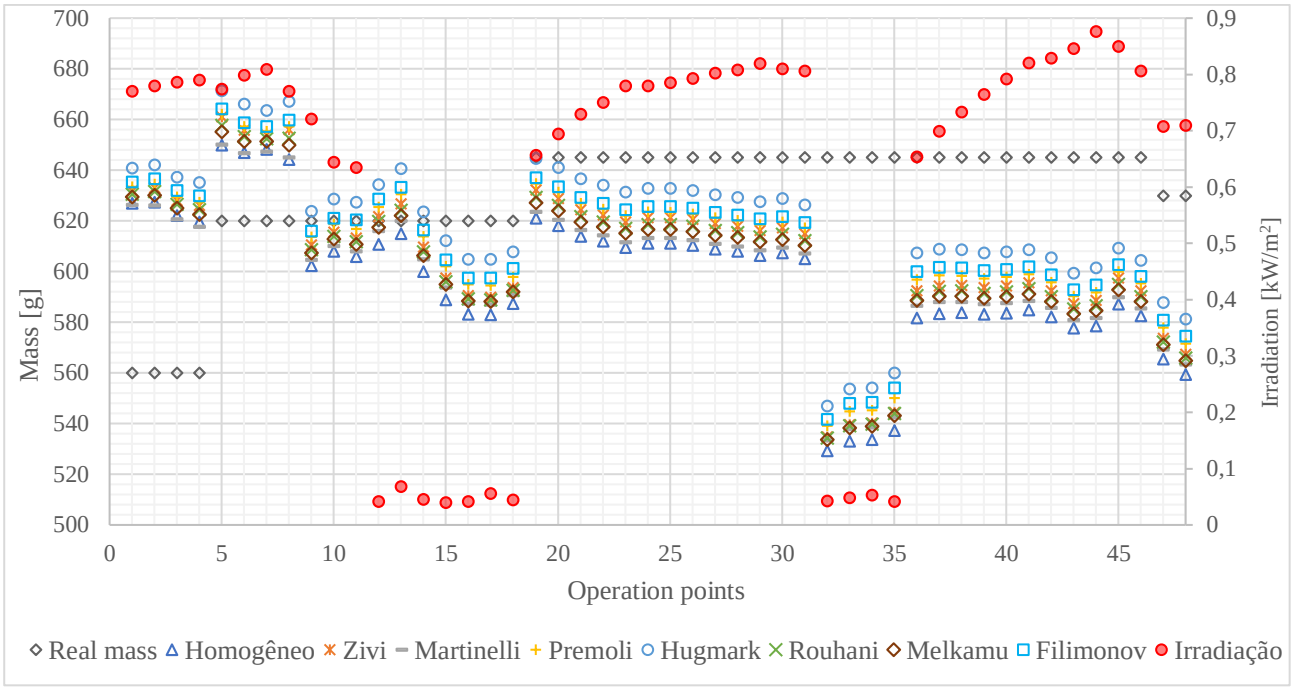

Figure 6 - Mass calculated for each void fraction correlation as a function of solar irradiation.

The effect of the variation of masses in the gas cooler and evaporator (through the Hughmark (1965) correlation) as a function of the low-pressure can be seen in Fig. 7.

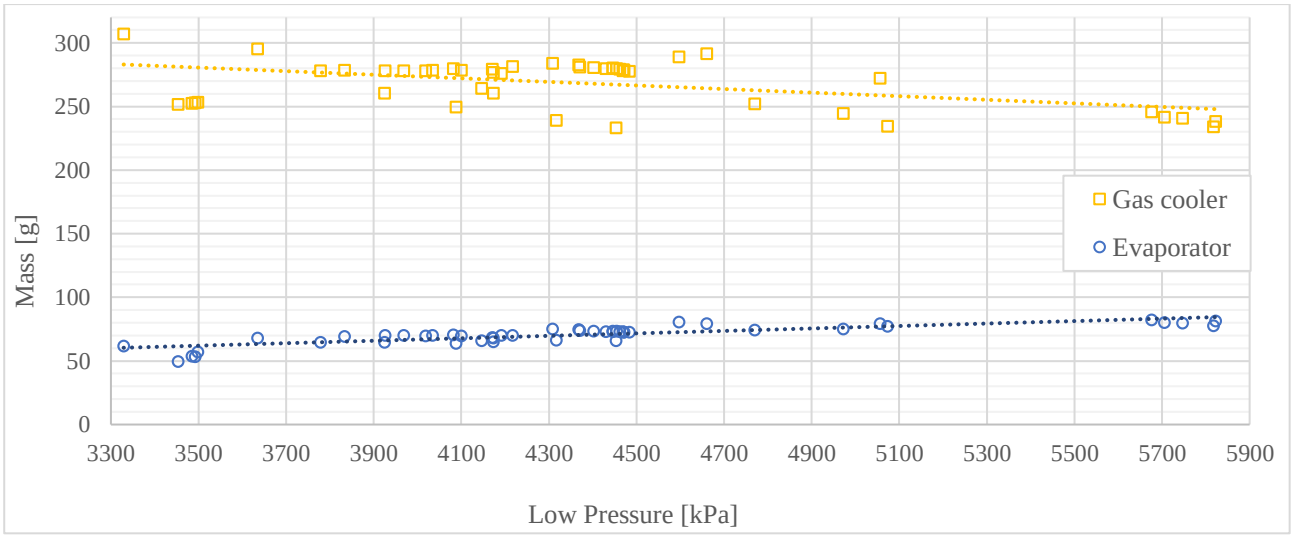

Figure 7 - Masses in the solar evaporator and gas cooler as a function of low-pressure.

Figure 8 distributes the model results for each tested correlation around the error ranges obtained from the experimental mass. In this graph, it is observed that all the mass values obtained by the model were within a tolerance range between + 15% and -18%.

As shown in Fig. 9, the best results for mass prediction were obtained by the correlations of Hughmark (1965) and Filimonov (1957), with an average error, in absolute terms, of 5.53% and 6.03% respectively.

In Fig. 10, considering a tolerance margin of ± 2%, the Hughmark (1962) correlation obtains the best result, with a total accuracy of 27.1% of the predictions against 14.6% achieved by the correlations of Zivi (1964), Premoli (1974) and Filimonov (1957). Expanding this margin to ± 5%, the correlations of Hughmark (1965), Zivi (1964), Premoli (1974) and Filimonov (1957) have a hit rate of 47.9%. With a margin of ± 10%, all correlations exceed the 80% range, except for the homogeneous model, which reached 75%. In a tolerance range of ± 15%, all correlations exceed the value of 90%, emphasizing Hughmark (1965), which reaches practically 98%. In ± 18%, all tested correlations reach the 100% correct mark each.

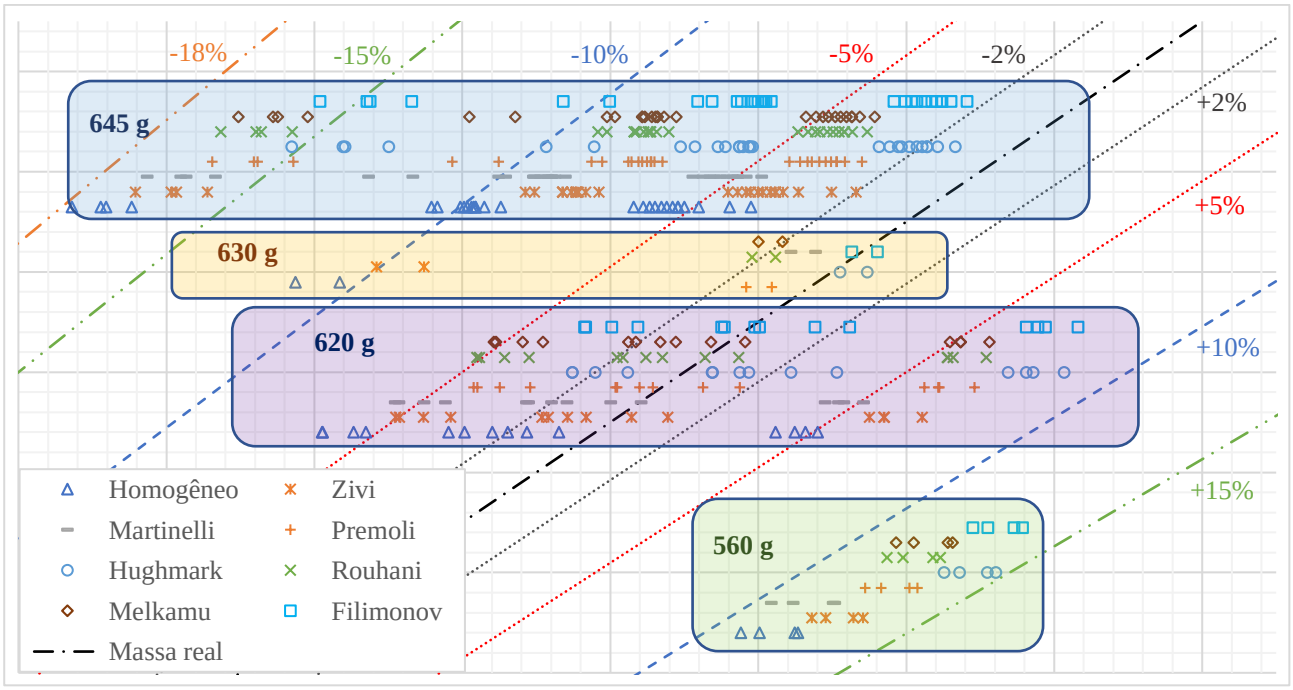

Figure 8 - General mapping of the masses calculated by the void fraction correlations.

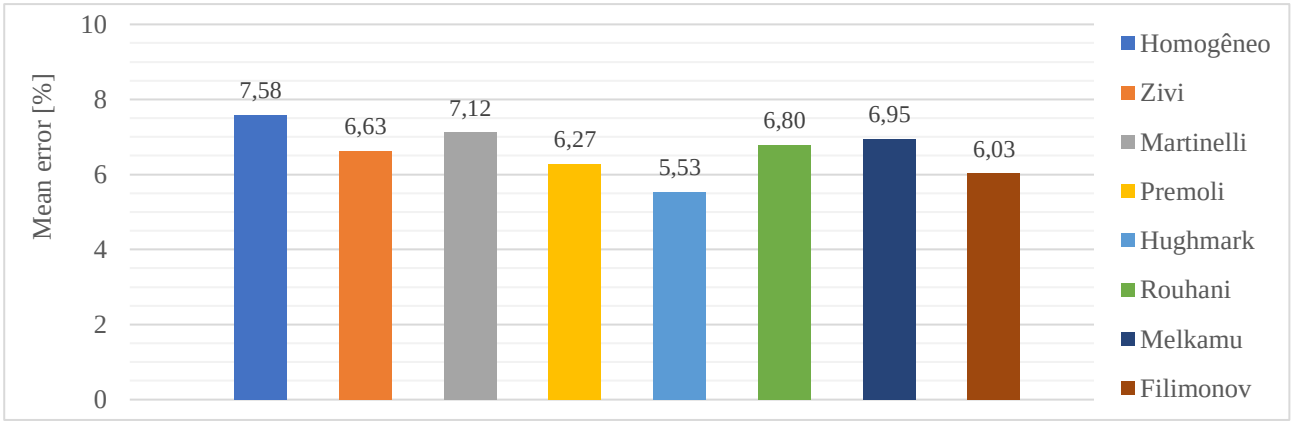

Figure 9 - Errors obtained for each void fraction correlation.

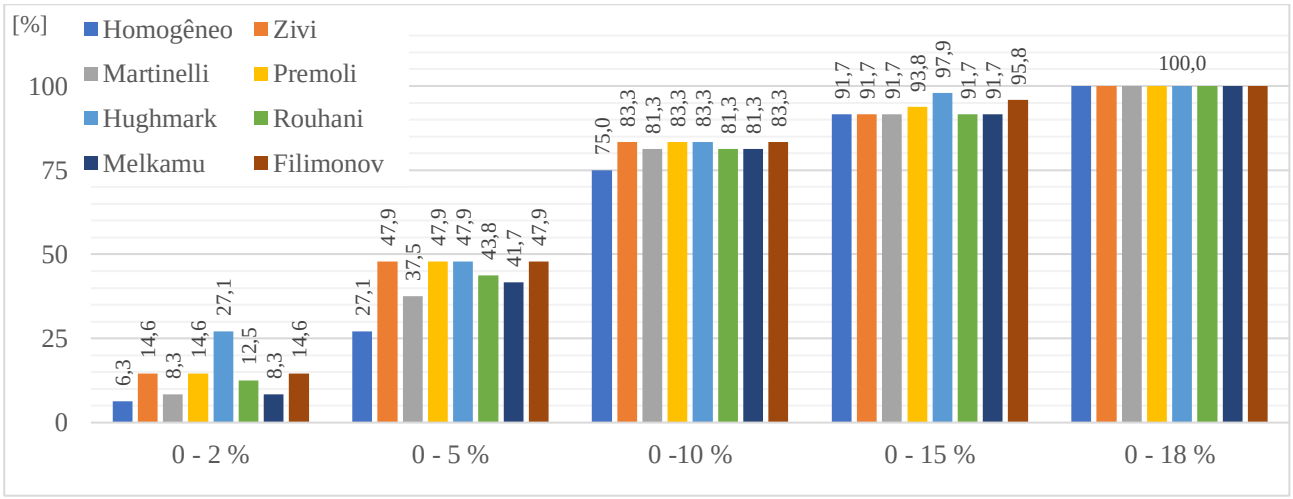

Figure 10 - Results of the void fraction correlations organized by tolerance ranges.

5. CONCLUSIONS

Solar irradiation directly affects the pressures and temperatures in the evaporator, which are proportional to the level of this irradiation. In the gas cooler, the pressure is not affected by the radiation level, nevertheless, the temperature at the compressor outlet also increases as the irradiation increases.

The level of irradiation influences the amount of mass predicted by the simulation model. In its absence, the model foresees smaller amounts of mass due to the decrease in the density of the refrigerant fluid in the solar evaporator, caused by the reduction of pressure. However, in the presence of sunlight, the total mass calculated by the model tends to decrease with increasing irradiation. This is due to the effect of reducing the density at the compressor outlet, under the effect of increasing the fluid temperature.

The best results found for predicting the mass of DX-SAHP were obtained by the correlations of Hughmark (1965) and Filimonov (1957), with an average error of 5.53% and 6.03% respectively. Considering a tolerance margin of ± 2%, the Hughmark (1965) correlation was successful in 27.1% of the predictions, and in ± 18%, all correlations were 100% accurate.

6. ACKNOWLEDGEMENTS

This work was supported by Foundation for Research Support of the State of Minas Gerais (FAPEMIG), National Council for Scientific and Technological Development (CNPq) and Coordination of Improvement of Higher Level Personnel (CAPES).

7. NOMENCLATURE

A	area (m^2)
c_p	specific heat constant pressure (kJ kg^{-1} K^{-1})
d	diameter (m)
f	friction factor
Fr	Froude number
G	mass flux ($kg.s^{-1}m^{-2}$)
g	gravity acceleration (m s^{-2})
H	heat transfer coefficient ($W.K.m^{-2}$)
h	enthalpy (kj kg^{-1})
I	Irradiation (W m^{-2})
k	Thermal conductivity (W m^{-1} K^{-1})
L	length (m)
m	mass (g)
$\dot{m}$	mass flow (kg s^{-1})
Nu	Nusselt number
P	pressure (bar)
Pr	Prandtl number
$\dot{Q}$	heat transfer rate (W)
Re	Reynolds number
S	Net radiation absorbed (W m^{-2})
T	temperature (°C)
U	global heat transfer coefficient (W K^{-1} m^{-2})
U_S	superficial velocity
V	volume (m^3)
We	Weber number

Greek letters

x	vapor quality
α	void fraction
γ	slip ratio
ϵ	emissivity
η	efficiency
ρ	density (kg m^{-3})
μ	viscosity (Pa s)
σ	superficial tension (N m^{-1})
σ_{SB}	Stefan-Boltzmann (5,67 x 10^8 W m^{-2} K^{-4})
ΔT_m	logarithmic mean temperature difference (°C)
χ	Martinelli parameter

Subscribed

ar	air
av	average
$cond$	condensation
$conv$	convection
ex	external
h	hydraulic
in	internal
i	input
l	liquid refrigerant
n	control volume
o	output
pc	critical point
rad	radiation
sat	saturation
t	total
T_C	critical temperature
sc	super critical
sd	super dense
v	vapor refrigerant
w	water

8. REFERENCES

Aprea, C.; Greco, A.; Maiorino, A. An experimental study on charge optimization of a trans-critical CO_2 cycle. Int. J. Environ. Sci. Technol. (2015) 12:1097–1106 DOI 10.1007/s13762-014-0502-6.

Çengel, Y.A. and Ghajar, A.J. (2015) Heat and Mass Transfer Fundamentals & Applications. 5th. New York: McGraw-Hill Education, 2015.

Churchill, S. W.; Chu, H. H. S. Correlating equations for laminar and turbulent free convection from a vertical plate. International Journal of Heat and Mass Transfer, v. 18, n. 11, p. 1323–1329, 1975.

Collier, John G. Convective boiling and condensation. Londres: Mc-Graw-Hill, 1972.

Duffie, J; Beckman, W. Solar Engineering of Thermal Process. 4. ed. Canada: Wiley, 2013.

Filimonov, A.I., Przhizhalovski, M.M., Dik, E.P., Petrova, J.N., 1957. The driving head in pipes with a free interface in the pressure range from 17 to 180 atm. Teploenergetika 4, 22–26.

Gnielinski, V., "New equations for heat and mass transfer in turbulent pipe and channel flow", International Chemical Engineering, vol. 16, pp. 359-368, 1976.

Hughmark, G.A. (1965), Holdup and heat transfer in horizontal slug gas-liquid flow, Chemical Engineering Science, Vol. 20, pp. 1007-1010.

Kong, X., Li, Y., Lin, L. and Yang, Y., 2017. "Modeling evaluation of a direct-expansion solar-assisted heat pump waterheater using R410A". International Journal of Refrigeration, Vol. 76, pp. 136–146.

Lockhart, R.; Martinelli, R. C. Proposed correlation of data for isothermal two-phase, two-component flow in pipes. Chemical Engineering Progress, v. 45, n. 1, p. 39-48, 1949.

Melkamu A., M. Woldesemayat and A.J. Ghajar (2007). Comparison of void fraction correlations for different flow patterns in horizontal and upward inclined pipes, International Journal of Multiphase Flow. Vol. 33, pp. 347–370.

Montagner, G. P. Um estudo da aplicação de ciclos transcríticos de CO_2 em sistemas comerciais de refrigeração. Tese (Doutorado). Programa de Pós-Graduação em Engenharia Mecânica. UFSC, Santa Catarina, 2013.

Premoli, A., Francesco, D. & Prina, A. (1971). A dimensionless correlation for determining the density of two-phase mixtures. Lo Termotecnica, (25) 17-26.

Rice, C. K., The effect of void fraction correlation and heat flux assumption on refrigerant charge inventory predictions, ASHRAE Transactions: Technical And Symposium Papers Presented at the 1987 Winter Meeting. New York, NY.

Revellin, R. Prediction of frictional pressure drop during flow boiling of refrigerants in horizontal tubes: Comparison to an experimental database, International Journal of Refrigeration, 2009.

Rohsenow, W. M. Heat Transfer and Temperature Distribution in Laminar Film Condensation, Trans. ASME, 78, pp. 1645-1648, 1956.

Rouhani, S. Z. and Axelsson, E. (1970), Calculation of void volume fraction in the sub cooled and quality boiling regions, International Journal of Heat Mass Transfer, Vol.13, pp. 383-393.

Shah, M. M. 2017, Unified correlation for heat transfer during boiling in plain mini/micro and conventional channels. International Journal of Refrigeration, Elsevier, v. 74, p. 604–624.

Steiner, D., 1993, "Heat Transfer to Boiling Saturated Liquids," VDI -Warmeatlas (VDI Heat Atlas), Editor: Ingenieure, V. D., VDI-Gessellschaft Verfahrenstechnik und Chemie-in-genieurwesen (GCV).

Yoon, S. H, et al. Heat transfer and pressure drop characteristics during the in-tube cooling process of carbon dioxide in the supercritical region. International Journal of Refrigeration, Elsevier, v. 26, p. 857–864, 2003.

Zhang, D., Wu, Q., Li, J. and Kong, X., 2014. "Effects of refrigerant charge and structural parameters on the performanceof a direct-expansion solar-assisted heat pump system".Applied Thermal Engineering, Vol. 73, No. 1, pp. 522 – 528.

Zivi, S. Estimation of steady-state steam void-fraction by means of the principle of minimum entropy production. Journal of Heat Transfer, v. 86, n. 2, p. 247-251, 1964. ISSN 0022-1481.

9. RESPONSIBILITY NOTICE

The authors are the only responsible for the printed material included in this paper.

10. APPENDICES 1 - MATHEMATICAL CORRELATIONS

Gnielinski (1976) Heat transfer coefficient. Single-phase fluid.	$$H = \frac{(f/8)\cdot(Re-1000)\cdot Pr}{1+12{,}7\cdot(f/8)^{(1/2)}\cdot(Pr^{(2/3)}-1)}\cdot\frac{k}{d_h}$$	(A1)
Yoon (2003) Heat transfer coefficient. Supercritical fluid.	$$Nu = aRe_a^b Pr_b^c\left(\frac{\rho_{pc}}{\rho}\right)^{y_n} \quad a=0{,}14;\ b=0{,}69;\ c=0{,}66\ e\ y_n=0\ se\ T>T_{pc}$$ $$a=0{,}013;\ b=1;\ c=-0{,}05\ e\ y_n=1{,}6\ se\ T_{pc}\le T$$	(A2)
Correlation of Shah (2017) Heat transfer coefficient. Boiling.	$$H = MAX\begin{cases}1{,}8B_1^{-0{,}8}B_3H_l\\ 230B_o^{0{,}5}B_3H_l\\ B_2B_o^{0{,}5}exp(2{,}74B_1^{-0{,}1})B_3H_l\\ B_2B_o^{0{,}5}exp(2{,}74B_1^{-0{,}15})B_3H_l\end{cases}$$ $$C_o=\left(\frac{1-x}{x}\right)^{0{,}8}\left(\frac{\rho_v}{\rho_l}\right)^{0{,}5} \quad B_1=\begin{cases}C_o\ se\ horizontal\ com\ Fr_l\ge 0{,}04\ ou\ vertical\\ 0{,}38C_oFr_l^{-0{,}3}\ se\ horizontal\ com\ Fr_l<0{,}04\end{cases}$$ $$B_2=\begin{cases}14{,}7 & B_o\ge 0{,}0011\\ 15{,}4 & B_o<0{,}0011\end{cases} \quad B_3=\begin{cases}2{,}1-0{,}008We_v-110B_o & B_3\ge 1\\ 1 & B_3<1\ ou\ Fr_l<0{,}01\end{cases}$$	(A3)
Churchill e Chu (1975) Heat transfer coefficient. Natural convection for inclined plates.	$$Nu=\left\{0{,}825+\frac{0{,}387Ra_L^{1/6}}{[1+(0{,}492/Pr)^{9/16}]^{8/27}}\right\}$$ Replace g by $g\cos\theta$ for $0<\theta<60°$	(A4)
Nusselt (1916) modified by Rohsenow (1956) Heat transfer coefficient. Condensation.	$$H_{cond}=H_v[\cos\theta]^{1/4}$$ $$H_v=0{,}943\left[\frac{g\rho_l(\rho_l-\rho_v)h_{lv}k_l^3}{\mu_l(T_{sat}-T_m)L}\right]^{1/4} \quad H_{lv}=h_{lv}+0{,}68c_{pl}(T_{sat}-T_m)$$	(A5)
Collier (1972) Head loss. Two-phase flow.	$$\frac{\partial P}{\partial z}=-G^2\frac{d}{dz}\left[\frac{x^2v_v}{\alpha}+\frac{(1-x)^2v_l}{1-\alpha}\right]-g\sin\theta\,[\alpha\,\rho_v+(1-\alpha)\,\rho_l]+\left(\frac{\partial P}{\partial z}F\right)$$	(A6)
Lockhart-Martinelli (1949) Separated Flow Model.	$$\left(\frac{\partial P}{\partial z}F\right)=\left(\frac{\partial P}{\partial z}F\right)_{lo}\phi_{lo}^2=\frac{f_{lo}\,v_l\,G^2\,(1-x)^2}{2\,d}\,\phi_{lo}^2 \quad \phi_{lo}^2=1+\frac{C}{\chi}+\frac{1}{\chi^2}$$ C *depends on the flow regime*	(A7)
Void Fraction Correlations		
Homogeneous Model	$$\alpha=\left[1+\left(\frac{1-x}{x}\right)\left(\frac{\rho_v}{\rho_l}\right)\right]^{-1}$$	(A8)
Zivi (1964)	$$\alpha=\left[1+\left(\frac{1-x}{x}\right)\left(\frac{\rho_v}{\rho_l}\right)\gamma\right]^{-1} \quad sendo, \quad \gamma=(\rho_l/\rho_v)^{1/3}$$	(A9)
Domansky e Didion (1983)	$$\alpha=(1+\chi^{0{,}8})^{-0{,}378}\quad com\quad \chi\le 10; \qquad \alpha=0{,}823-157\,ln\,\chi\quad com\quad \chi>10$$	(A10)
Premoli (1971)	$$\alpha=\left[1+\left(\frac{1-x}{x}\right)\left(\frac{\rho_v}{\rho_l}\right)\gamma_P\right]^{-1} \quad \gamma_P=1+a[y(1+yb)^{-1}-yb]^{0{,}5} \quad y=\left(\frac{x}{1-x}\right)\left(\frac{\rho_l}{\rho_v}\right)$$ $$a=1{,}578Re_l^{-0{,}19}(\rho_l/\rho_v)^{0{,}22} \quad b=0{,}0273We_lRe_l^{-0{,}51}(\rho_l/\rho_v)^{-0{,}08}$$	(A11)
Hughmark (1965)	$$\alpha=\left[1+\left(\frac{1-x}{x}\right)\left(\frac{\rho_v}{\rho_l}\right)\gamma\right]^{-1}.K_{Hugmark}$$ $$Z=\left[G.d\left(\mu_l+\alpha(\mu_v-\mu_l)\right)^{-1}\right]^{1/6}\left\{(g.D)^{-1}\left[Gx\left(\rho_v\alpha_{hom}(1-\alpha_{hom})\right)^{-1}\right]^2\right\}^{1/8}$$	(A12)
Rouhani modified by Steiner (1992)	$$\alpha=x\rho_v{}^{-1}\left[c\left(x\rho_v{}^{-1}+(1-x)\rho_l{}^{-1}\right)+1{,}18(1-x)[g\sigma(\rho_l-\rho_v)]^{0{,}25}(G\rho_l{}^{-0{,}25})^{-1}\right]^{-1}$$ $$c=1+0{,}12(1-x)$$	(A13)
Melkamu (2007)	$$\alpha=U_{S,v}/\left\{U_{S,v}\left(1+\frac{U_{S,l}}{U_{S,v}}\right)^{\left(\frac{\rho_g}{\rho_l}\right)^{0{,}1}}+2{,}9\left[\frac{gd\sigma(1+\cos\theta)(\rho_l-\rho_g)}{\rho_l^2}\right]^{0{,}25}(1{,}22+1{,}22\sin\theta)^{\frac{P_{atm}}{P}}\right\}$$ $$U_{S,v}=\mu_v\frac{Re_v}{\rho_v d} \quad U_{S,l}=\mu_l\frac{Re_l}{\rho_l d}$$	(A14)
Filimonov (1957)	$$\alpha=U_{S,v}/\left[(U_{S,l}+U_{S,v})+S_d\right] \quad S_d=(0{,}65-0{,}0385P)\left(\frac{d_h}{0{,}063}\right)^{0{,}25} \quad P<12{,}7Mpa$$ $$S_d=(0{,}33-0{,}00133P)\left(\frac{d_h}{0{,}063}\right)^{0{,}25} \quad P\ge 12{,}7Mpa$$	(A15)